Available online at www.sciencedirect.com
ScienceDirect
Journal of Power Sources 159 (2006) 171–178
JOURNAL OF POWER SOURCES
www.elsevier.com/locate/jpowsour

Nano-ionics in the context of lithium batteries

P. Balaya*, A.J. Bhattacharyya, J. Jamnik, Yu.F. Zhukovskii, E.A. Kotomin, J. Maier

Max Planck Institute for Solid State Research, D-70569 Stuttgart, Germany

Available online 6 June 2006

Abstract

In this paper, we highlight the field of nano-ionics which in contrast to the well established field of nano-electronics is still in status nascendi. We present some of our recent findings of different physical phenomena in the field of nano-ionics with special emphasis in the context of lithium batteries, addressing the following anomalies in various properties: (a) enhanced storage, Coulombic efficiency and excess storage at low potential due to interfacial insertion reaction, (b) thermodynamic aspects giving rise to excess cell voltage and curved shapes instead of plateau regions during multiphase co-existence and (c) transport behavior in a new class of soft matter electrolytes that combines high ionic conductivities at room temperature with the favorable properties of 'soft matter'. Thus we emphasise here that the nano-ionics is relevant not only for fundamental science, but also important for technological applications.
© 2006 Elsevier B.V. All rights reserved.

Keywords: Nano-ionics; Lithium batteries; Interfacial storage; Soggy sand electrolytes

1. Introduction

Nano-size effects currently receive considerable attention both in experimental as well as in theoretical respect not only due to their fundamental significance but also in view of potential applications. An often cited example is the change of thermodynamic stability, for example, the suppression of the melting point in the case of nano-sized Au particles by several hundreds of degrees which is due to the excess surface free energy of the small particles according to [1]:

$$\mu_{\mathrm{MX}}(\mathrm{nano}) = \mu^{\infty}_{\mathrm{MX}} + \left(\frac{2\bar{\gamma}}{\bar{r}}\right) V \tag{1}$$

where $\bar{\gamma}$ is the average surface tension, $\bar{r}$ the average radius and V is the partial molar volume, here identical with the volume of MX.

A variety of size effects on transport phenomena are primarily discussed in the context of electronic materials. The most striking example is the quantum confinement in nano-electronics [2,3]. In the present article, we stress such nano-size effects in ionic materials and present some of the recent findings of different physical phenomena in the field of nano-ionics with special emphasis in the context of lithium batteries, addressing anomalies in storage, thermodynamics and transport properties.

2. Energetics of nanoparticles

A major size effect on the energetics of nano-particle is due to the excess surface contribution given by Eq. (1). Very few experiments have been carried out to estimate this excess contribution in the case of the nanoparticles. Among them, the excess surface enthalpy measured using calorimetry experiments on nanoparticles of alumina and titania by the group of Navrotsky are worth mentioning [4,5]. Electrochemical e.m.f. measurements are also known to provide thermodynamic data in fact enthalpy and entropy if measured as a function of temperature [6–8]. Recently, we have measured the excess surface enthalpy as well as surface entropy contributions of rutile nanoparticles of different sizes, 100 and 25 nm, by an electrochemical e.m.f. cell using Na-β″ alumina as solid electrolyte in the temperature range 250–450 °C.

Both electrodes of the cell consist of a composite of $Na_2Ti_6O_{13}$, rutile and gold powder separated by Na-β″ alumina [9]. While the reference electrode contains bulk rutile of 2 μm, the working electrode comprises nanoparticles of either 100 or 25 nm. To a first approximation the e.m.f. is related to the Gibbs free energy of coarsening through the Nernst equation by

$$\left(\frac{2\bar{\gamma}}{\bar{r}}\right) V = -nFE \tag{2}$$

It has however to be pointed out that in e.m.f. method the experimentally accessible interfacial contributions stem from

* Corresponding author. Tel.: +49 711 689 1725; fax: +49 711 689 1722.
E-mail address: s.weiglein@fkf.mpg.de (P. Balaya).

0378-7753/$ – see front matter © 2006 Elsevier B.V. All rights reserved.
doi:10.1016/j.jpowsour.2006.04.115

the electrode particles at the electrode/electrolyte interface [8]. The advantage of the present electrochemical cell is that the e.m.f. which is measured directly provides the difference of the Gibbs free energies of formation ($\Delta_f G^\circ$) of the titania crystals on both sides. A stable excess e.m.f. of about 62 mV was obtained at 621 K for the nano-sized rutile of 25 nm versus 2 μm bulk rutile [10]. Unlike single component silver nanoparticles, that grow with time due to an electrochemical Ostwald ripening (because of highly mobile Ag^+) leading to an unstable e.m.f. values [8], this stable excess e.m.f. in the case of binary system such as rutile (TiO_2) nanoparticle, has its origin in the low mobility of the electrochemically inactive constituents.

3. Transport behavior of nanostructured materials

Nano-structuring has significant influence on the transport behavior of ionic as well as mixed conductors [11,12]. This has been shown quite clearly for cases in which space charges at the interface play a predominant role as regards to the electrical conduction [13–15]. We consider two basic situations, one for the accumulation and the other for the depletion of space charges and their respective influences on the electrical conduction.

3.1. Accumulation of space charges

A master example for the accumulation of space charges and its influence on the ionic conductivity had been given by Sata et al. [16] in the case of BaF_2/CaF_2 multilayers. It was shown that the experimental results can consistently be explained by a redistribution of the segregation of F^- ions at the core of BaF_2/CaF_2 interfaces, leading to enhanced vacancy and interstitial contributions. As long as the thickness of each layer L is larger than the Debye screening length λ, the trivial size effects occur leading to the nominal increase in conductivity. At tiny spacing space charge layers are expected to overlap leading to non-trivial size effects that results in locally varied conductivities.

3.2. Depletion of space charges

Let us consider the space charge depletion and refer to acceptor doped $SrTiO_3$, the electrical properties of which is well investigated [17–20]. In this case, the grain boundaries have been found to be positively charged and hence accompanied by zones in which the concentrations of electron holes ($h^\bullet$) and oxygen vacancies ($V_o^{\bullet\bullet}$) are diminished. Thus the stoichiometry in grain boundary zones is grossly different from the bulk stoichiometry. As a result of such depletion effects, the impedance spectra exhibit two semicircles, one at high frequencies due to bulk and the other at low frequencies due to the blocking grain boundary (depletion layers). Recently we investigated the frequency dependence of real and imaginary parts of the complex impedance on microcrystalline (2500 nm) and nanocrystalline (80 nm) (Fe-doped) $SrTiO_3$ samples [21]. Two relaxation times are clearly identified for the microcrystalline $SrTiO_3$ (2500 nm). In nanocrystalline $SrTiO_3$ on the other hand only a single relaxation time referring to the low frequency signal remains. Thus unlike microcrystalline $SrTiO_3$ exhibiting both bulk and semi-infinite interfacial contributions to conduction, in nanocrystalline $SrTiO_3$ the bulk contribution disappears and space charge effects are observed throughout. The Debye length is deduced to be larger than the grain size, thus confirming the appearance of a mesoscopic phenomenon where the depleted space charges overlap within the grains [21]. This phenomenon is the counterpart to the accumulation layer overlap discussed in literature [16,22] but occurs at much larger spacing owing to a lack of screening (depletion of carriers) and the larger dielectric constant.

Different nano-size effects have been predicted so far based on the influence of particle size on different components of the electrochemical potential [23] given by the expression:

$$\tilde{\mu}_j = \mu_j^0 + RT \ln c + RT \ln \gamma + z_j e \Phi \quad (3)$$

where the standard term μ_j^0 refers to the chemical free energy of forming an isolated carrier j, c the concentration and Φ is the electrical potential ($z_j e$: charge of a single carrier); the activity coefficient γ corrects for energetic or entropic excess effects in non-dilute systems. So far, we have discussed the effects related to the energetics and the transport behavior. The following section focuses on size effects related to the energy storage particularly in the context of lithium batteries.

4. Lithium batteries

4.1. Nanocrystalline electrodes

In most of the commercial applications, lithium (Li) batteries use rocking chair cells [4,5] with $LiCoO_2$ and C as the positive and negative electrodes respectively and have the advantages of both excellent cyclic performance and a Coulombic efficiency that exceeds 95%. However, such a homogeneous storage process suffers from a low storage capacity resulting in a low energy density (120–150 Wh kg^{-1}). Most of today's high-performance portable microelectronic devices demand a high energy density. A novel way of lithium storage was introduced by the group of Tarascon [24,25] to achieve high lithium storage in several transition metal oxide compounds using a reversible conversion reaction that involves heterogeneous lithium storage. Such a conversion reaction for the transition metal oxide CoO, transforms it into Co/Li_2O nanocomposite upon incorporation of 2 Li^+, in addition an extra storage of 0.6 Li^+ occurs at low potential resulting in an enhanced storage capacity of nearly 900 mAh g^{-1}. However it was noticed that upon first charging only about 70% of Li^+ could be extracted from Li_2O, i.e., the Coulombic efficiency during first charge is about 70%. Most of the materials studied so far [24–27] exhibits only 70–80% of lithium extraction during the first cycle, the remaining 20–30% is lost permanently within the Li_2O host matrix.

We have shown recently, that RuO_2 as an electrode material exhibits not only high lithium storage capacity of 1110 mAh g^{-1} but also nearly 100% Coulombic efficiency [28]. Fig. 1 presents the complete charge–discharge curve of RuO_2 versus Li in the voltage window 0–4.3 V. The size of the initial RuO_2 particle is in the range of 30–200 nm. High resolution transmission elec-

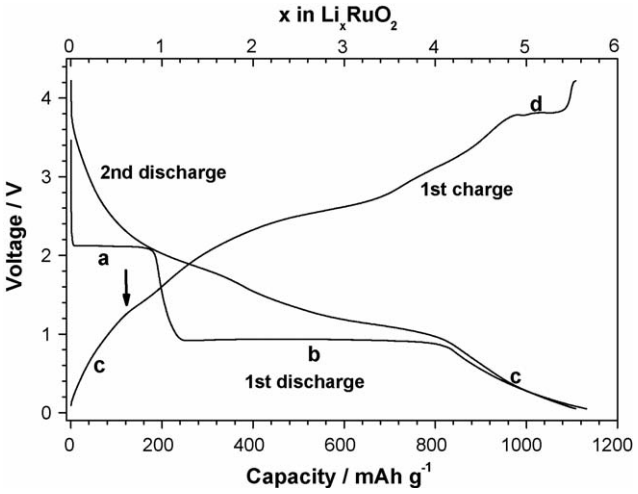

Fig. 1. Electrochemical curve for the RuO_2/Li cell over the voltage window 0–4.3 V. Reprinted with permission from Ref. [28].

tron microscopy (HRTEM) and selected area electron diffraction (SAED) images (refer also Fig. 3b) for a fully lithiated (5.6 Li) RuO_2 revealed a nanocomposite microstructure of Ru/Li_2O covered by a thick solid electrolyte interface (SEI) film (about 5 nm). On complete re-oxidation, corresponding to a potential of 4.3 V, the SEI film disappears completely and nanocrystalline RuO_2 reforms upon extraction of 5.5 Li [28]. That is on insertion of 5.6 Li, the initial RuO_2 phase disappears and on extraction of 5.5 Li, the RuO_2 phase with crystallite size of 2–5 nm is formed again. Obviously, 99% Coulombic efficiency is achieved even when the cycling is limited to the 0.8–4.3 V range. This indicates that the decomposition and reformation of RuO_2 described by Eq. (4) is highly reversible and not influenced by the growth of SEI and other reactions (discussed later) in the sloped region:

$$RuO_2 + 4Li^+ + 4e^- \rightleftarrows Ru + Li_2O \quad (4)$$

One possible explanation for the complete extraction of Li^+ from the Ru/Li_2O nanocomposite is the excellent inherent transport behavior of the decisive phases being in the nano-scale (2–5 nm). It is known that RuO_2 is a metallic conductor at room temperature with the highest electronic conductivity among all oxides and exhibits a reasonably high Li^+ diffusion coefficient [29]. Preliminary measurements using thermogravimetry have also shown that RuO_2 can easily be made non-stoichiometric suggesting that the oxygen defects are indeed significantly mobile. Thus the favourable mass and charge transport properties of RuO_2 along with short transport lengths (2–5 nm) seems to facilitate the complete extraction of Li from Ru/Li_2O nanocomposite.

4.2. Cell voltage and shape of the curve

Nano-size results in an excess cell voltage that can be estimated by Eq. (1), discussed earlier in the energetics of nanomaterials. For a grain size of 1 nm, $\bar{\gamma}$ being about 0.1 J m^{-2} and V assumed to be 25 cm^3 mole^{-1}, the cell voltage may be modified by about 100 mV [30].

In general, different storage mechanisms will result in different charging–discharging curves. Since these curves usually are affected by overpotentials due to kinetic reasons, we assume here that the charging rates are very small, such that the curves can be considered on a thermodynamic basis. For convenience let us focus on an electrode material enabling a reversible conversion reaction. Then we may expect three storage mechanisms (also consult Fig. 6): (i) in the first stage Li will homogeneously be inserted into bulk. The corresponding charge–discharge curve will be slightly sloped due to the entropy part and the interaction terms of the Li chemical potential (anomalies are possible due to structural transitions). (ii) As the saturation limit is reached, the conversion reaction takes place. In this regime the charge–discharge curve is flat (a non-vanishing slope possible due to nano-size effects, see Eq. (1)). (iii) After the completion of the conversion reaction, a further storage is possible due to the presence of interfaces. This storage mechanism, which will be explained in the next section, yields a capacitor like charging–discharging curves.

Note here the consequences of the Gibbs–Kelvin term for the Li chemical potential:

$$\mu_{Li}(\bar{r}) = \mu_{Li}(\bar{r} \to \infty) + 2\left(\frac{\bar{\gamma}(\bar{r})}{\bar{r}}\right)_{Li} V_{Li} \quad (5)$$

First a variation in that term can cause a sloped discharge–charge curve even in (macroscopically) non-variant situations, second according to a constancy of $\mu_{Li}(\bar{r})$ within the nanocrystalline electrode, a composition variation occurs as a consequence of a grain size distribution [30].

5. Interfacial lithium storage

5.1. Extra storage at low potential

It is to be noticed that the Li-storage capacities in RuO_2 corresponding to the sloped voltage regions during first discharge and charge processes are about 330 and 120 mAh g^{-1} respectively (refer Fig. 1). After the first discharge, if the voltage is limited within 0–1.2 V, a quite reversible Li-storage behavior with a capacity of 120 mAh g^{-1} is observed (Fig. 2) at a rate of $C/5$ (discharge in 45 min). Moreover the storage at low potential can be achieved even with a high rate performance for example, 70 mAh g^{-1} could be stored at a rate of 4C (discharge in 1.3 min) in the case of Ru/Li_2O [31,32]. Thus the storage behavior within this voltage window (0–1.2 V) resembles that of a capacitive behavior with a good cyclic performance and high rate performance.

A similar extra storage of lithium has been observed in many other composites such as Co/Li_2O, Ni/Li_2O, Fe/Li_2O, Ti/LiF, etc. Thus the extra storage at low potential is indeed a commonly observed phenomenon in most of the oxides and fluorides studied so far [24,26]. The pseudo-capacitive behavior observed in Co/Li_2O nanocomposite during the charge–discharge at low potential has been tentatively explained by a reaction of lithium with the conducting-type polymeric film formed in situ [33]. Fig. 3 presents the HRTEM images of RuO_2 electrode mate-

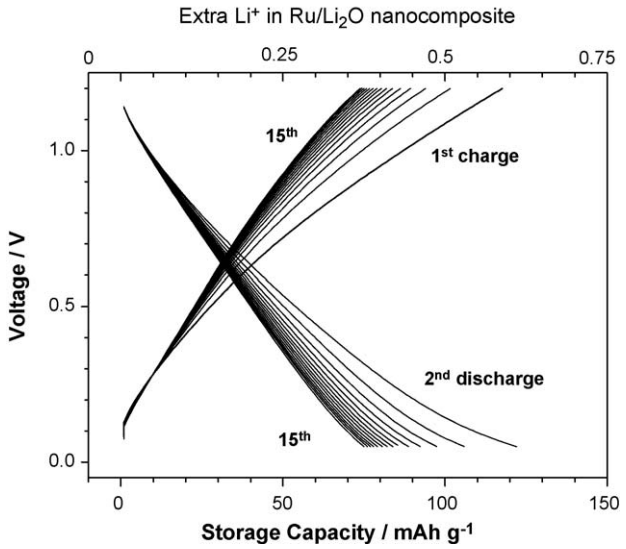

Fig. 2. Electrochemical charge–discharge curves for the Ru/Li_2O nanocomposite within the voltage window 0–1.2 V. Reprinted from Ref. [32] with permission.

rial for the incorporation of 4 Li^+ (0.8 V) and 5.6 Li^+ (0.02 V) during discharge and ex-corporation of 0.6 Li^+ (1.2 V) during charge. It is clear from these images that the SEI film is mainly formed in the sloped region on discharge, retained nearly the same thickness on charging until 1.2 V and starts decomposing beyond the sloped region (1.2 V) in particular at and above 3.8 V (refer Fig. 1, plateau d). This means that the Li-storage during the discharge in the sloped region (Fig. 1) cannot only be attributed to the reaction with the SEI formation. Another explanation given in the literature [34] is the segregation of metal at the interface/grain boundaries and subsequent alloy reaction of metal with the incorporated lithium. This possibility is however ruled out in the present case of the Ru/Li_2O nanocomposite, as no alloy reaction has been known between Ru and Li metals. As both Ru (generally speaking metal) and Li_2O cannot store lithium, it is believed that the storage at low potential is caused by a two-phase effect. We proposed recently an interfacial charge storage mechanism in which an excess lithium is accommodated in the boundary regions via charge separation between nanosized metal and Li_2O grains until the lithium potential approaches the value of pure Li [30]. Thus while the tentative explanation to this extra Li storage by Laruelle et al. [31] refers to the formation and decomposition of conducting component of SEI at the outer region of the particle, present explanation due to interfacial storage mechanism refers to the extra storage which occur at the interface of metal and Li_2O nanocrystallites.

5.2. *Interfacial lithium storage: phenomenological model*

In order to understand the particle size effect on lithium storage capacity of a composite which consists of pure ionic and of pure electronic conductor, we consider a simplified geometry, e.g. a heterostructure: metal/Li_2O/metal (see Fig. 4a, metal is denoted by the dashed lines located at $x = 0$ and $x = L$). We consider such a structure essentially as a supercapacitor, and model the storage capacity as a function of the interfacial spacing L. We

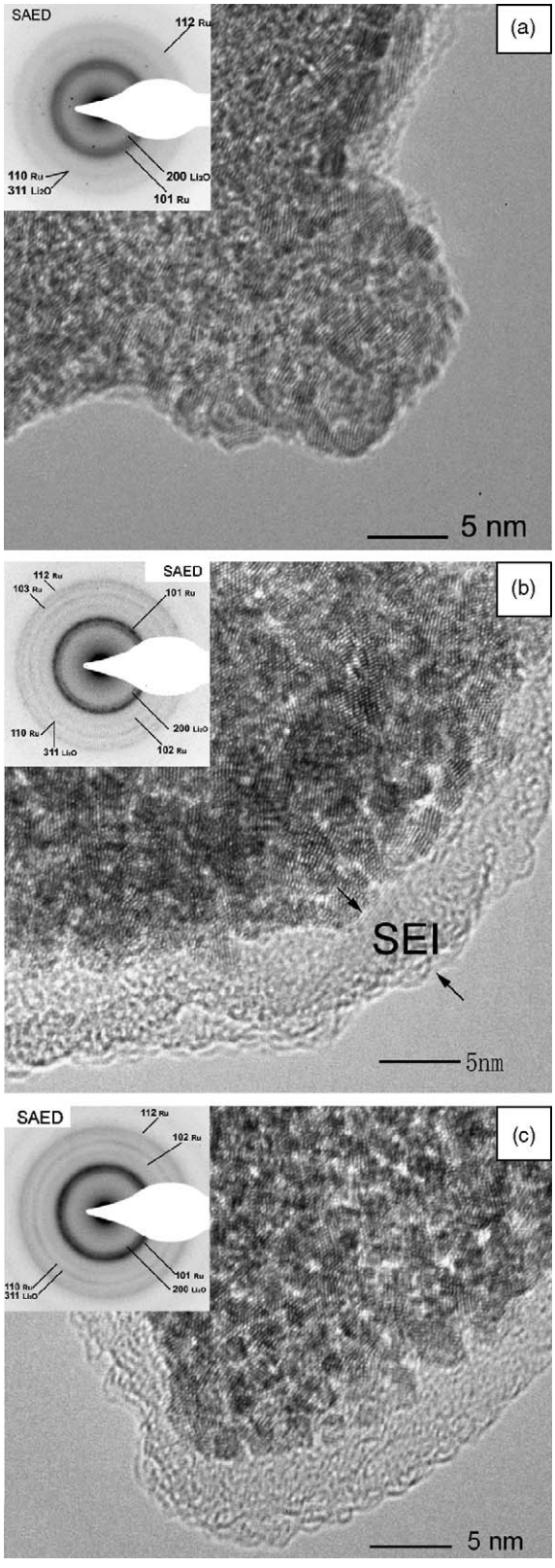

Fig. 3. HRTEM image for RuO_2/Li cell with (a) 4 Li^+ incorporated – discharged to 0.8 V, (b) 5.6 Li^+ incorporated – discharged to 20 mV and (c) 0.6 Li^+ excorporated – charged to 1.2 V. Reprinted with permission from Ref. [28].

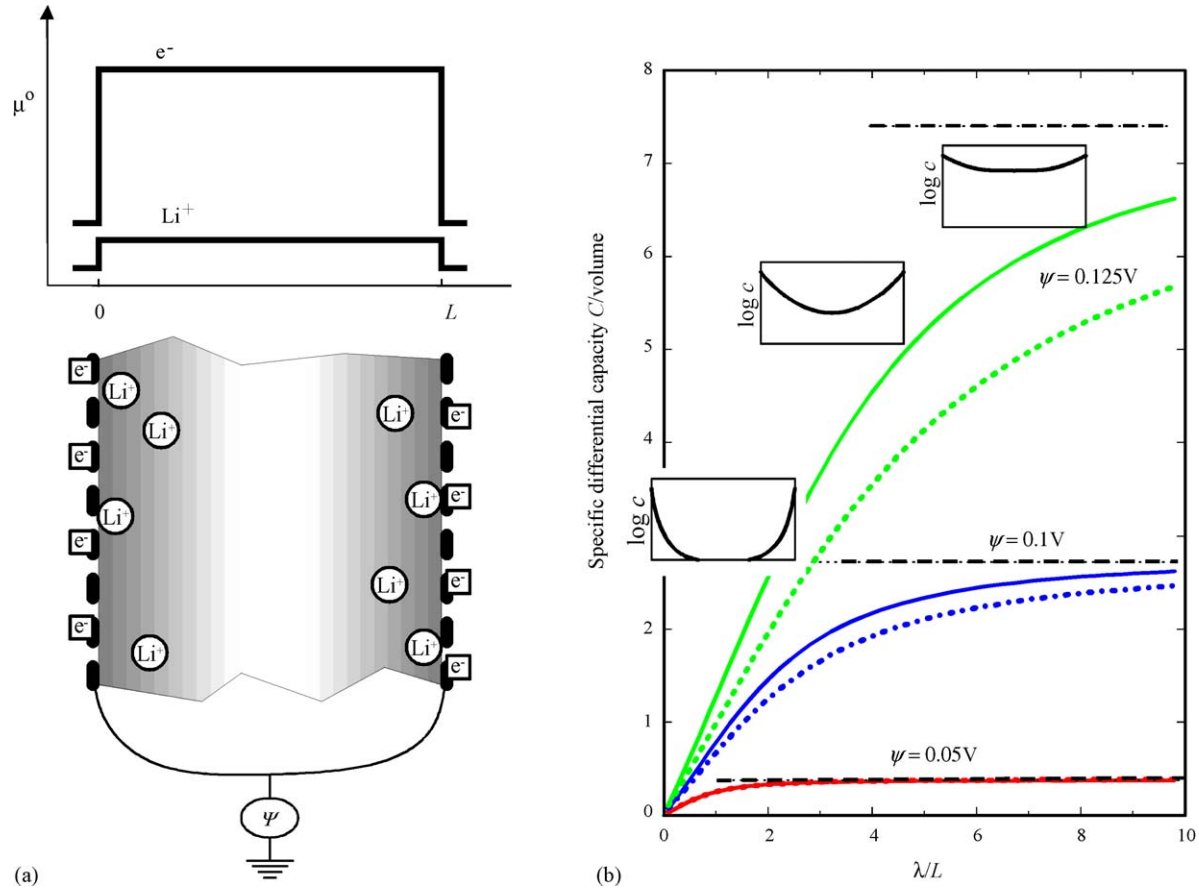

Fig. 4. (a) Schematics of the heterostructure metal/ionic conductor/metal, which was used in calculations. The electrodes are at potential Ψ (vs. Li) and permeable for Li^+ ions. (b) Predictions of the simple space charge model. Differential capacity normalized per heterostructure volume as a function of the reciprocal interfacial spacing is given. Three pairs of curves refer to three different space charge potentials assumed. Solid curves refer to an ideal lattice gas approximation. Dotted curves of the same color refer to a more realistic situation in which finite ion-size is taken into account. Flat dotted lines denote the capacity in a hypothetical case in which conventional Li insertion is assumed (the ionic conductor is replace by a mixed conductor). Reprinted with permission from Ref. [30].

assume a dilute defect situation, such that simple space charge model can be applied.

Fig. 4 b shows the calculated differential capacity for different applied voltages as a function of the inverse interfacial spacing. Please note, that the capacity is normalized per volume, and not per electrode area as usual in the case of electrostatic energy storage. As expected, for spacing large compared to the Debye length, we obtain a linear dependence. At smaller spacing, however, the curves flatten and reach a saturation value, which is close to the value expected in the case of homogeneous storage (insertion). Moreover, the capacity becomes proportional to the electrode volume, rather than the interfacial area. This feature is typical for chemical storage of energy and demonstrates that at small interfacial spacing the difference between a capacitor and a battery is getting blurred [30].

This mechanism is rather different from the homogeneous storage i.e., in $LiCoO_2$ where Li and hence both Li^+ and e^- are inserted into a host lattice. The interfacial storage mechanism can be illustrated with the help of Fig. 5. In Li_2O for e.g., the Li solubility within the bulk or grain boundary (7) is – owing to its pronounced redox stability – negligible in spite of the availability of interstitial sites for Li^+. At the contact to a metal, however, Li^+ can be accommodated at the Li_2O side of the boundary

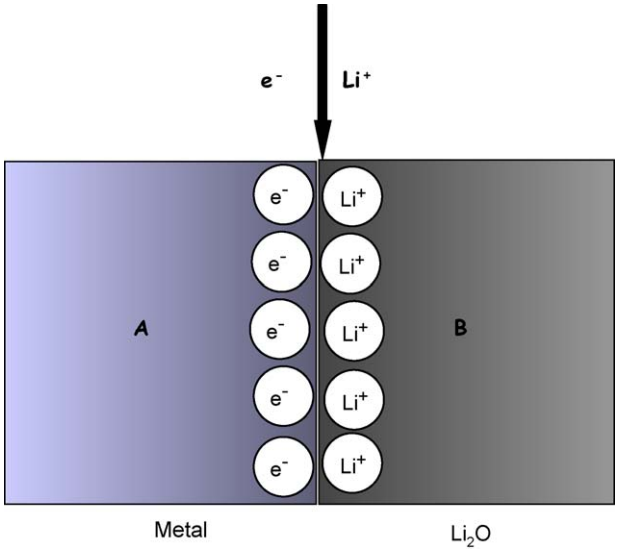

Fig. 5. Schematic representation of the interfacial storage according to the phenomenological model described here.

while the electrons are restricted to the metal side. In short, at contacts of two phases A and B at which e^- can be stored in A and the Li^+ in B as shown in Fig. 5, we expect an interfacial storage.

5.3. Ab initio calculations at the Ti/Li_2O model interface

In order to check these ideas, ab initio hybrid DFT-HF B3PW calculations [35] were performed for the Li_2O/Ti interface. Although it is known that TiO_2 cannot be electrochemically reduced to metal, the Li_2O/Ti interface has been chosen here as a *model* interface mainly due to a proper lattice matching and absence of irregular structures and steps at the interface. The Li_2O/Ti interface is modeled by a slab infinite in two dimensions and containing six (1 1 1) planes of Li_2O, in contact with one or two Ti (0 0 0 1) planes. Here the discussion is briefly for the case of Ti interface with the Li terminated Li_2O slab. A more interesting case of oxygen termination is being investigated at the moment.

We considered different positions of inserted Li atoms, positions at the slab surface opposite to the Ti/Li_2O interface, positions at octahedral interstitial sites inside the slab, and finally at the interface between Ti and Li_2O slab. Self-consistent calculations in this special case show a considerable electron transfer from excess Li atoms towards Ti atoms if it is close to the interface. More details on this first principles calculations are published elsewhere [32].

In short, the complete electrochemical behavior of the cell RuO_2 versus Li during first discharge within the voltage window 0–4.3 V comprises three regimes, one which is due to the formation of $LiRuO_2$ and corresponds to a volume insertion, a second one that refers to the formation of Ru/Li_2O nanocomposite via a conversion reaction and finally an extra storage regime at the low potential along the sloped region that we explained by the interfacial storage. Fig. 6 illustrates these three reaction mechanisms and the variation of relevant chemical potential that gives rise to different cell voltages [30].

6. Soggy sand electrolytes

This section elucidates the role of nanomaterials and interfacial effects in liquid environment. Previously the quantitative concept of 'Heterogeneous Doping' has been considered in the context of solid composite electrolytes such as AgCl/Al_2O_3 [11]. In the present context, the above concept has been successfully applied to non-aqueous salt solutions to generate a new class of electrolytes viz. "soggy sand" electrolytes [36] which combine high ionic conductivities at room temperature (higher than commercial liquid electrolytes) with favorable properties of "soft matter". These electrolytes, which hold considerable potential for application in electrochemical devices [37], typically comprise of dispersions of fine inorganic acidic oxide particles e.g. SiO_2, TiO_2 in non-aqueous Li-salt solutions e.g. $LiClO_4$, $LiPF_6$, in model solvents such as methanol (MeOH), or Li-battery relevant solvents like ethylene carbonate (EC) or dimethyl carbonate (DMC). The name "soggy sand" is derived from the fact that in the regime of high conductivities the composite possesses a soft matter consistency similar to that of "soggy" sand.

The composite conductivity has been found to be dependent on several parameters viz. surface acidity of oxides, volume fraction and particle size, solvent dielectric constant, salt concentration and temperature. Dispersion of oxide particles varying in surface acidity–basicity e.g. SiO_2, TiO_2, Al_2O_3 (size ≈300 nm) in 0.1 M $LiClO_4$ in MeOH ($\varepsilon_r = 32.6$) resulted in a remarkable variation in overall composite conductivity. Starting from pure solution ionic conductivity, the conductivity was observed to be enhanced up to a maximum of half an order in magnitude. Similar enhancements in ionic conductivity were also observed by dispersing SiO_2 (size: 7–40 nm) in commercial Li-battery electrolytes e.g. $LiPF_6$ in EC:DMC (v/v, 1:1). This striking ion conductivity enhancement is analogous to the situation for weak solid electrolytes. In such case, internal adsorption of an ion takes place at the insulator surface e.g. of F^- in PbF_2–SiO_2 resulting in the formation of a defect-rich space charge layer at the conductor–insulator interface. In the present scenario of

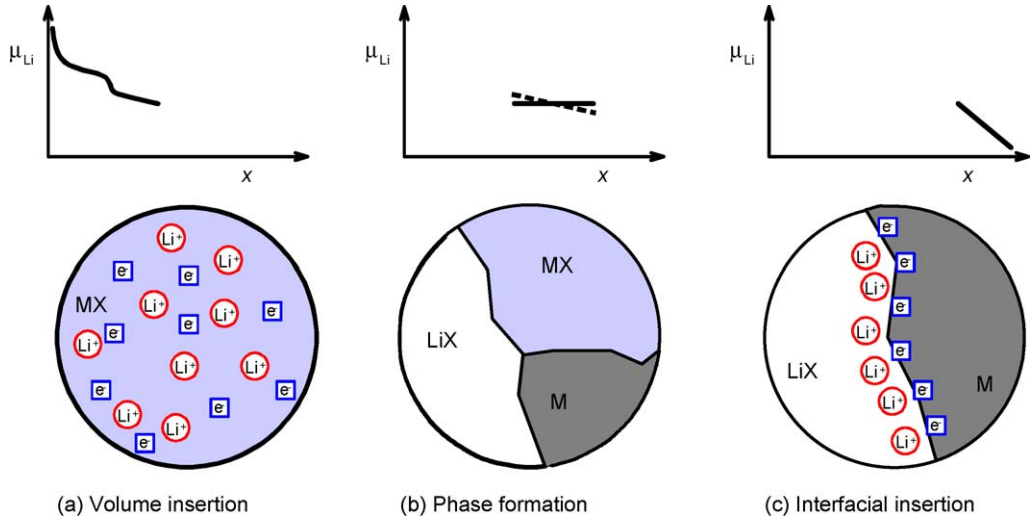

Fig. 6. Charge storage mechanisms in electrode particle by means of (a) insertion reaction; (b) and (c) interfacial reaction associated with charge separation. In (b) solely ions and (c) solely electrons are injected into the particle. Reprinted with permission from Ref. [30].

non-aqueous solutions introduction of oxides results in dissociation of ion-pairs (ion-pair concentration very high in pure solution as $\varepsilon_{\text{non-aq. solvent}} < \varepsilon_{\text{water}}$) and depending on the surface acid–base property of the added oxide, anions or cations are adsorbed on the surface leading to a high counter-ion (Li^+) concentration in the vicinity of the oxide (space charge layer). Composite with acidic oxides (e.g. SiO_2) were shown to be more efficient in trapping anions at the surface than basic oxides (e.g. Al_2O_3), which is well confirmed by more negative measured ζ–potential value for SiO_2 (−48 mV) compared to Al_2O_3 (−37 mV).

An important feature in the conductivity variation with oxide volume fraction is the observation of a percolation-type behavior typically observed for composite systems in which ion conduction predominantly occurs via interfaces. Such a behavior has been extensively discussed for solid–solid composites [38] where an increase in conductivity is in agreement with the appearance of a first percolation threshold (formation of percolating pathways) and the decrease after the maximum with the appearance of a second percolation threshold (blockage of percolating pathways by insulator particles). At low volume fractions no noticeable ionic conductivity enhancement was observed due to the dominance of the double layer repulsion over percolation. The onset in percolation i.e. the volume fraction at which an attractive network is established throughout the composite [39] depends on a variety of parameters. The onset seems to appear at lower φ (≈0.07) for basic oxides compared to acidic oxides ($\varphi \approx 0.15$) [36] due to lower surface density of adsorbed charges. Similar differences can also be observed for different solvents (e.g. THF $\varepsilon_r = 7.4$). With the exception of a few systems, it is a special feature that the conductivity steeply falls after the maximum. So far, we attribute the unexpectedly early blocking (i.e. value of φ at which $\sigma_m = 0$) to severe wetting inhomogeneities [39].

Apart from the enhanced ionic conductivity, the mechanical properties are worth mentioning. The high effective viscosity of the "soggy sand" electrolytes endows them with improved mechanical strength (in terms of partial shapeability) compared to liquid electrolytes in the assembly of an electrochemical cell. We investigated the galvanostatic charge–discharge behavior of "soggy sand" electrolytes at 25 °C in cell configurations without a typical polymer separator (e.g. Celgard^{TM}). Fig. 7(a) and (b) shows the excellent electrochemical performance of soggy sand with graphite and $LiFePO_4$, respectively. The high constancy in capacity over few tens of cycles implies that "soggy sand" electrolytes do not have any detrimental effect towards lithium.

Thus with the extension of Heterogeneous Doping to non-aqueous liquid electrolytes, we have generated a new class of electrolytes. We have also demonstrated the applicability to electrochemical devices e.g. lithium batteries based on special mechanical property.

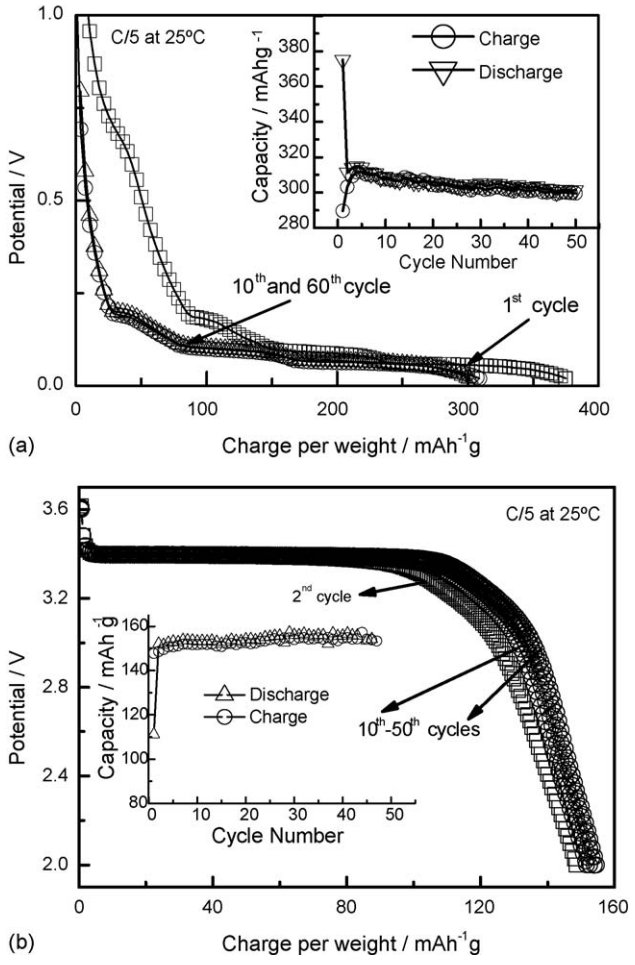

Fig. 7. Room temperature electrochemical performance of the cell (a) Graphite|$LiPF_6$/$LiCF_3SO_3$ in EC/DMC (v/v, 1:1):SiO_2 $\varphi = 0.04$ |Li and (b) $LiFePO_4$|$LiPF_6$/$LiCF_3SO_3$ in EC/DMC (v/v, 1:1):SiO_2 $\varphi = 0.04$|Li using soggy sand electrolyte. $LiFePO_4$ was supplied by the group of J.M. Tarascon at Amiens, France [37].

7. Conclusions

In this article, we have emphasised that nano-ionics is relevant not only for fundamental science, but also important for technological applications. It is shown that the nanocrystalline electrodes exhibit both high theoretical capacity as well as high Coulombic efficiency. A novel interfacial lithium storage mechanism which is a consequence of nanocrystallinity has been discussed to explain the extra storage at low potential. In addition, "soggy sand electrolytes" are discussed representing a new class of soft matter electrolytes that demonstrates the use of interfacial effects in liquid systems.

Acknowledgements

Authors thank N. Sata, H. Li, M. Dolle, J. Fleig and S. Hore for useful discussions. We also thank L. Kienle for providing the HRTEM images.

References

[1] Ph. Buffat, J.-P. Borel, Phys. Rev. A 13 (1976) 2287.
[2] X.L. Wu, J.Y. Fan, T. Qiu, X. Yang, G.G. Siu, P.K. Chu, Phys. Rev. Lett. 94 (2005) 026102.

[3] (a) F. Rosei, J. Phys. Condens. Matter 16 (2004) S1373;
(b) E.L. Brus, J. Chem. Phys. 80 (1984) 4403;
(c) Y. Wang, H. Herron, J. Phys. Chem. 95 (1991) 525.
[4] M.R. Ranade, et al., PNAS 99 (2002) 6476.
[5] J.M. McHale, A. Auroux, A.J. Perrota, A. Novrotsky, Science 277 (1997) 788.
[6] P. Knauth, G. Schwitzgebel, A. Tschöpe, S. Villain, J. Solid State Chem. 140 (1998) 295.
[7] K.T. Jacob, K.P. Jayadevan, R.M. Mallya, Y. Waseda, Adv. Mater. 12 (2000) 440.
[8] A. Schroeder, J. Fleig, D. Gryaznov, J. Maier, W. Sitte, J. Phys. Chem. B (2006), in press.
[9] M. Holtzinger, J. Maier, W. Sitte, Solid State Ionics 86 (1996) 1055.
[10] P. Balaya, J. Maier, Electrochem. Solid State Lett. (2006), in preparation.
[11] J. Maier, Prog. Solid State Chem. 23 (1995) 171.
[12] H.L. Tuller, Solid State Ionics 131 (2000) 143;
J. Schoonman, Solid State Ionics 135 (2000) 5;
J. Maier, Z. Phys. Chem. 217 (2003) 415.
[13] P. Knauth, H.L. Tuller, Solid State Ionics 136 (2000) 1215.
[14] A. Tschöpe, Solid State Ionics 139 (2001) 267;
S. Kim, J. Maier, J. Electrochem. Soc. 149 (2002) J73.
[15] W. Puin, S. Rodewald, R. Ramlau, P. Heitjans, J. Maier, Solid State Ionics 131 (2000) 159.
[16] N. Sata, K. Eberman, K. Eberl, J. Maier, Nature 408 (2000) 946.
[17] R.A. De Souza, J. Fleig, J. Maier, O. Kienzle, Z. Zhang, W. Sigle, M. Rühle, J. Am. Ceram. Soc. 86 (2003) 922.
[18] I. Denk, J. Claus, J. Maier, J. Electrochem. Soc. 144 (1997) 3526.
[19] Z.L. Zhang, W. Sigle, F. Phillipp, M. Ruhle, Science 302 (2003) 846.
[20] X. Guo, J. Fleig, J. Maier, J. Electrochem. Soc. 148 (2001) J50.
[21] P. Balaya, J. Jamnik, J. Fleig, J. Maier, Appl. Phys. Lett. 88 (2006) 062109.
[22] J. Maier, Solid State Ionics 23 (1987) 59.
[23] J. Maier, Nat. Mater. 4 (2005) 805.
[24] P. Poizot, S. Laruelle, S. Grugeon, L. Dupont, J.-M. Tarascon, Nature 407 (2000) 496.
[25] A. Debart, L. Dupont, P. Poizot, J.-B. Leriche, J.-M. Tarascon, J. Electrochem. Soc. 148 (2001) A1266.
[26] H. Li, G. Richter, J. Maier, Adv. Mater. 15 (2003) 736;
H. Li, P. Balaya, J. Maier, J. Electrochem. Soc. 151 (2004) A1878.
[27] F. Badaway, N. Pereira, F. Cosandey, G.G. Amatucci, J. Electrochem. Soc. 150 (2003) A1209.
[28] P. Balaya, H. Li, L. Kienle, J. Maier, Adv. Func. Mater. 13 (2003) 621.
[29] M. Armand, F. Dalard, D. Deroo, C. Mouliom, Solid State Ionics 15 (1985) 205.
[30] J. Jamnik, J. Maier, Phys. Chem. Chem. Phys. 5 (2003) 5215.
[31] P. Balaya, M. Dolle, H. Li, J. Maier, in preparation.
[32] Yu.F. Zhukovskii, P. Balaya, E.A. Kotomin, J. Maier, Phys. Rev. Lett. 96 (2006) 058302.
[33] S. Laruelle, S. Grugeon, P. Poizot, M. Dolle, L. Dupont, J.-M. Tarascon, J. Electrochem. Soc. 149 (2002) A627.
[34] L.Y. Beaulieu, D. Larcher, R.A. Dunlap, J.R. Dahn, J. Electrochem. Soc. 147 (2000) 3206.
[35] V.R. Saunders, R. Dovesi, C. Roetti, R. Orlando, C.M. Zicovich-Wilson, N.M. Harrison, K. Doll, B. Civallieri, I.J. Bush, Ph. D'Arco, M. Llunell, CRYSTAL-03 User Manual, University of Turin, Italy, 2003.
[36] A.J. Bhattacharyya, J. Maier, Adv. Mater. 16 (2004) 811, and references therein.
[37] A.J. Bhattacharyya, M. Dollé, J. Maier, Electrochem. Solid State Lett. 7 (2004) A432.
[38] A. Bunde, W. Dieterich, H.E. Roman, Phys. Rev. Lett. 55 (1985) 5.
[39] A.J. Bhattacharyya, J. Maier, R. Bock, F.F. Lange, Solid State Ionics, 2005, communicated.